# Understanding Interfacial Segregation in Polymer Blend Films with Random and Mixed Side Chain Bottlebrush Copolymer Additives

Hao Mei, §,a Jyoti P. Mahalik, §,b,c Dongjoo Lee, a Travis S. Laws,d Tanguy Terlier,e Gila E. Stein,d Rajeev Kumar,\*c Rafael Verduzco\*af

<sup>a</sup>Department of Chemical and Biomolecular Engineering, Rice University, Houston, TX 77005

<sup>b</sup>Department of Polymer Science and Engineering, University of Massachusetts, Amherst, MA
01003

<sup>c</sup>Center for Nanophase Materials Sciences, Oak Ridge National Laboratory, Oak Ridge, TN 37830

<sup>d</sup>Department of Chemical and Biomolecular Engineering, University of Tennessee, Knoxville,

TN 37996

<sup>e</sup>SIMS Lab, Shared Equipment Authority, Rice University, Houston, TX 77005

<sup>f</sup>Materials Science and NanoEngineering, Rice University, Houston, TX 77005

Email: rafaelv@rice.edu, kumarr@ornl.gov

§These authors contributed equally

### **ABSTRACT:**

Bottlebrush polymers are complex macromolecules with tunable physical properties dependent on the chemistry and architecture of both the side chains and the backbone. Prior work has demonstrated that bottlebrush polymer additives can be used to control the interfacial properties of blends with linear polymers but has not specifically addressed the effects of bottlebrush side chain microstructures. Here, using a combination of experiments and self-consistent field theory (SCFT) simulations, we investigated the effects of side chain microstructures by comparing the segregation of bottlebrush additives having random copolymer side chains with bottlebrush additives having a mixture of two different homopolymer side chain chemistries. Specifically, we synthesized bottlebrush polymers with either poly(styrene-ran-methyl methacrylate) side chains or with a mixture of polystyrene (PS) and poly(methyl methacrylate) (PMMA) side chains. The bottlebrush additives were matched in terms of PS and PMMA compositions, and they were blended with linear PS or PMMA chains that ranged in length from shorter to longer than the bottlebrush side chains. Experiments revealed similar behaviors of the two types of bottlebrushes, with a slight preference for mixed side-chain bottlebrushes at the film surface. SCFT simulations were qualitatively consistent with experimental observations, predicting only slight differences in the segregation of bottlebrush additives driven by side chain microstructures. Specifically, these slight differences were driven by the chemistries of the bottlebrush polymer joints and side chain end-groups, which were entropically repelled and attracted to interfaces, respectively. Using SCFT, we also demonstrated that the interfacial behaviors were dominated by entropic effects with high molecular weight linear polymers, leading to enrichment of bottlebrush near interfaces.

Surprisingly, the SCFT simulations showed that the chemistry of the joints connecting the bottlebrush backbones and side chains played a more significant role compared with the side chain end groups in affecting differences in surface excess of bottlebrushes with random and mixed side chains. This work provides new insights into the effects of side chain microstructure on segregation of bottlebrush polymer additives.

KEYWORDS: bottlebrush copolymer; side chain; microstructure; entropy; joints.

# Introduction

In polymer blend thin films, the polymer composition near interfaces is generally different than that in the bulk. This difference arises due to a combination of enthalpic, <sup>1,2</sup> entropic, <sup>3–5</sup> and processing conditions, <sup>6–9</sup> preferentially driving some polymers towards the substrate and the air interface. Fundamental understanding of these effects is desired for tailoring and controlling the surface properties of polymeric materials for relevant applications including the development of antifouling coatings, <sup>10–12</sup> biocompatible surfaces, <sup>13</sup> and patterned surfaces. <sup>14</sup>

Numerous experimental and modeling studies have shown that architectural effects in polymer blends can drive enrichment of one component near an interface.<sup>5,15–31</sup> Wu and Fredrickson used self-consistent field theory (SCFT) to study architectural effects, and they showed that conformational entropy differences can drive branched or ring polymers towards interfaces in blends with chemically similar linear polymers. They also utilized a linear response theory for predicting density profiles near interfaces by accounting for enthalpic and entropic effects arising from chain ends, branch points, and middle segments.<sup>3</sup> Yethiraj used integral equation theory to account for packing effects in addition to conformational entropy differences in blends of star and linear polymers. This work demonstrated that packing entropy can drive linear polymers to the

immediate vicinity of the interface and conformational entropy drives enrichment of star polymers at distances corresponding to the length of the star polymer branches.<sup>32</sup> Wu, Foster, and coworkers employed neutron reflectivity measurements to study the enrichment of branched and ring polymers near interfaces when blended with linear polymers. They showed that a linear response theory accounting for the number of chain ends and branches was consistent with the experimental measurements for blends of branched and linear polymers.<sup>19</sup> However, enrichment in blends of linear and ring polymers could not be accounted for using a linear response theory, and neutron reflectivity experiments found enrichment or depletion depending on the molecular weight of the ring polymer in the blend. This crossover from depletion to enrichment with molecular weight was attributed to entropic packing effects.<sup>18</sup> Archer and coworkers developed a linear response theory for surface enrichment in blends of linear and branched polymers. They showed that surface tension measurements of pure components could be used to predict surface enrichment behaviors.<sup>27</sup>

In our own works, we examined thin film blends of bottlebrush polymers and linear polymers and found a broad range of conditions where bottlebrush polymers accumulate at surfaces and interfaces. 15,17,29 The surface activity of these additives was governed by a combination of enthalpic and entropic effects and, in some cases, non-equilibrium effects due to processing conditions. Introducing different side chain chemistries can be used to tune the energetics of interactions with the majority linear polymer in the blend and the energetics at the film interfaces. For example, work by Kim et al. utilized bottlebrush additives that segregated to film interfaces to control the orientation of microdomains. Bottlebrush copolymers and miktoarm copolymers to different side-chain chemistries can self-assemble into periodic domains, and

these topics have been recently reviewed along with other types of mixed-graft block copolymers.<sup>36</sup>

However, prior work primarily focused only on bottlebrush additives with side chain chemistries that either matched the linear polymer matrix or had a mixture of two different side chain chemistries. Bottlebrush polymers that contain either mixtures of side chain chemistries or random copolymer side chains, hereafter referred to as "mixed chain bottlebrush polymers" or "random bottlebrush polymers", respectively, are architecturally and chemically similar, but differ in the microstructure of the side-chains (**Figure 1**). This difference in the side chain microstructure may impact enrichment near interfaces, and understanding these differences can help in the design of additives for modifying surfaces and interfaces.

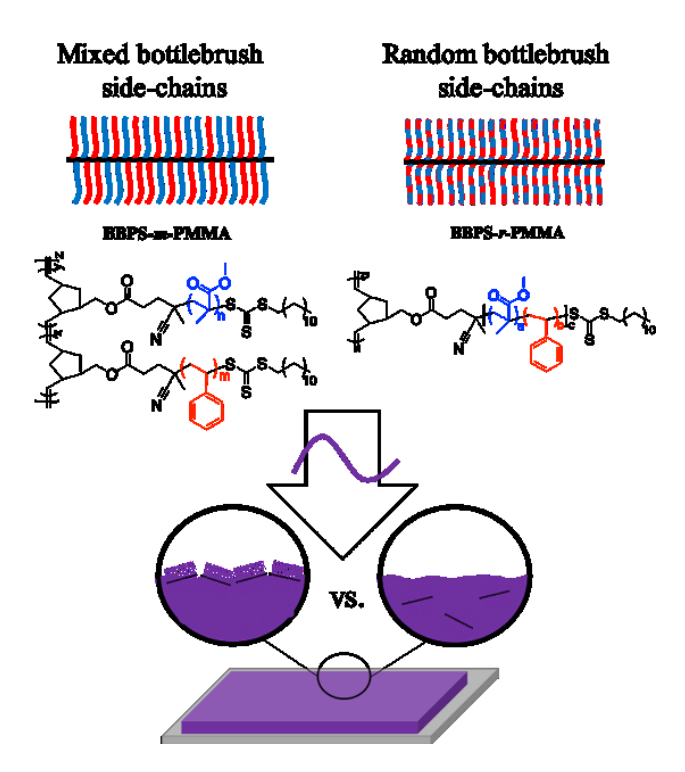


**Figure 1.** Molecular structures for mixed side chain (BBPS-*m*-PMMA) and random copolymer side chain (BBPS-*r*-PMMA) bottlebrush polymers along with schematics showing surface enrichment or depletion of the bottlebrush additive.

Herein, we studied surface enrichment in blends of linear polymers and mixed chain or random bottlebrush polymers (Figure 1). Our work focused on methyl methacrylate (MMA) and styrene (S) chemistries since these can be copolymerized to produce random copolymers. The mixed or random side chain bottlebrush polymers were blended with linear polystyrene (PS) or poly(methyl methacrylate) (PMMA) to investigate the vertical distributions of the bottlebrush additives and segregations towards film interfaces. We also performed self-consistent field theory (SCFT) simulations to understand the effects of side chain microstructures. Our experiments revealed subtle but measurable differences in the segregation of the mixed and random side-chain bottlebrushes, with a slight preference for mixed side-chain bottlebrushes at the film surface. SCFT simulations revealed that this could be understood as a balance between joint and side-chain end group chemistries, which were entropically repulsive and attractive towards interfaces, respectively. This study demonstrates that changes in the side chain microstructures provide subtle changes to the segregations towards interfaces and provides insights into the roles of side chain end group and joint chemistries in driving the segregation of branched polymer additives towards interfaces. This study also demonstrates that the segregation behaviors of both types of bottlebrush copolymer additives are similar, and the more versatile synthesis of bottlebrush polymers with mixed bottlebrush side chains provides an advantage over bottlebrush polymers with random copolymer side chains for the practical development of bottlebrush copolymer additives.

# **Experimental**

### Materials.

All chemical reagents were purchased from commercial sources and used as received unless noted otherwise. Silicon wafers were washed by Hellmanex III, deionized water, acetone and isopropyl alcohol with sonication for 15 minutes for each solvent. Then the wafers were treated with UV/ozone to remove contaminants. 2,2′-azobis(2-methylpropionitrile) (AIBN) was purified by recrystallization in methanol. Styrene was passed through an alumina column to remove inhibitor. The 3<sup>rd</sup> generation Grubbs catalyst ((H<sub>2</sub>IMes)(pyr)<sub>2</sub>(Cl)<sub>2</sub>RuCHPh)<sup>37</sup> and *exo*-5-nobornene-2-methanol (*exo*-NBOH)<sup>38</sup> were synthesized as previously reported. Linear PS polymers were purchased from Polymer Standard Service-USA Inc., and linear PMMA polymers were synthesized by anionic polymerization as described in our previous paper.<sup>29</sup>

((1S,2R,4S)-bicyclo[2.2.1]hept-5-en-2-yl)methyl-4-cyano-4-(((dodecylsulfanyl)carbonothioyl)-thio)-pentanoate (NBCTA). NBCTA was synthesized according to previous study.<sup>39</sup> <sup>1</sup>H nuclear magnetic resonance spectroscopy (<sup>1</sup>H NMR) analysis is presented in the **Supporting Information** Figure S1.

Norbornene functionalized polystyrene macromonomer (NBPS). NBPS was synthesized by reversible addition-fragmentation chain transfer (RAFT) polymerization as previously reported.<sup>29,40</sup> <sup>1</sup>H NMR and GPC analyses are presented in the **Supporting Information Figures S2** and **S6**, respectively.

Norbornene functionalized poly(methyl acrylate) macromonomer (NBPMMA). NBPS was synthesized as previously reported.<sup>29</sup> <sup>1</sup>H NMR and GPC analyses are presented in the **Supporting** Information Figures S3 and S6, respectively.

*PS-m-PMMA* bottlebrush copolymer (**BBPS-m-PMMA**). The bottlebrush copolymer with mixed PS and PMMA side chains was synthesized according to a previous study.<sup>29</sup> <sup>1</sup>H NMR and GPC analyses are presented in the **Supporting Information Figures S4** and **S6**, respectively.

Norbornene functionalized polystyrene and poly(methyl methacrylate) random macromonomer (NBPS-r-PMMA). NBPS-r-PMMA was synthesized by reversible addition-fragmentation chain transfer (RAFT) polymerization using methods similar to those previously reported. NBCTA (93.8 mg, 0.184 mmol), styrene (0.495 mL, 4.33 mmol), methyl methacrylate (1.20 mL, 11.33 mmol) and AIBN (3.00 mg, 0.0183 mmol) were dissolved in 2.19 mL anhydrous tetrahydrofuran (THF) in a Schlenk tube equipped with a stir bar. Three freeze-pump-thaw cycles were conducted to remove oxygen. Then the tube was heated to 80 °C to start the reaction. During the reaction, aliquots were taken and tested by gel permeation chromatography (GPC) to monitor the molecular weight. After reaching the target molecular weight, the reaction was stopped, and the polymer was precipitated in cold methanol and collected by filtration. After drying in a vacuum oven, the polymer was dissolved in DCM and reprecipitated in cold methanol to further purify the macromonomer. This purification process was repeated three times to completely remove unreacted monomers. Yield: 33.2 %. <sup>1</sup>H NMR and GPC analyses are presented in the Supporting Information Figures S5 and S7, respectively.

*PS-r-PMMA* random side chain bottlebrush copolymer (**BBPS-r-PMMA**). BBPS-r-PMMA was synthesized in a nitrogen filled glove box. NBPS-r-PMMA (137 mg, 0.042 mmol) was added into a vial with stir bar. Anhydrous DCM was added to the vial to target a total macromonomer

concentration of 0.05 M. Catalyst (H<sub>2</sub>IMes)(pyr)<sub>2</sub>(Cl)<sub>2</sub>RuCHPh was dissolved in the desired amount of anhydrous DCM and added into the macromonomer solution. After 12-hour reaction, the product was collected by precipitating in cold hexane. Yield: 69.6 %. GPC analyses is presented in the **Supporting Information Figures S7**.

**Scheme 1.** Synthetic scheme for the preparation of BBPS-*m*-PMMA and BBPS-*r*-PMMA. i) AIBN, MMA, THF, 80 °C; iii) AIBN, styrene, THF, 80 °C; iii) (H<sub>2</sub>IMes)(pyr)<sub>2</sub>(Cl)<sub>2</sub>RuCHPh, DCM; iv) AIBN, MMA, styrene, THF, 80 °C; v) (H<sub>2</sub>IMes)(pyr)<sub>2</sub>(Cl)<sub>2</sub>RuCHPh, DCM.

**Table 1.** Characteristics of macromonomers NBPS, NBPMMA and NBPS-r-PMMA and bottlebrush copolymers BBPS-m-PMMA and BBPS-r-PMMA.  $M_n$ : number-averaged molecular weight; D: molecular-weight dispersity; DP: degree of polymerization;  $N_{sc}$ : side chain degree of polymerization;  $N_b$ : backbone degree of polymerization; PS %: mass percentage of styrene repeat units of the overall content of styrene and methyl methacrylate repeat units.

	$M_n^{ m a} ({ m kg/mol})$	$D^{b}$	DP	$N_{sc}^{c}$	$N_b$	PS % <sup>d</sup>
NBPS	4.14	1.14	34.9			100 %
NBPMMA	4.13	1.24	36.1			0 %

NBPS-r-PMMA	3.25	1.25	26.9			47 %
BBPS-m-PMMA	179.7	1.35		35.5	43.5	47 %
BBPS-r-PMMA	173.9	1.60		26.9	53.5	47 %

<sup>&</sup>lt;sup>a</sup>determined by <sup>1</sup>H NMR for NBPS and NBPMMA and through GPC-LS analysis for bottlebrush copolymers; <sup>b</sup>determined by GPC; <sup>c</sup>represents an average of the PS and PMMA side chain DPs for BBPS-*m*-PMMA; <sup>d</sup>determined by <sup>1</sup>H NMR.

**Table 2**. Characteristics of polystyrene (PS) and poly(methyl methacrylate) (PMMA) linear homopolymers and blends of linear homopolymers with bottlebrush polymers.  $M_n$ : linear polymer number-average molecular weight;  $N_m$ : linear polymer degree of polymerization; D: linear polymer molecular weight dispersity;  $N_m/N_{sc}{}^m$ : ratio of linear polymer degree of polymerization to that of the BBPS-m-PMMA side chains;  $N_m/N_{sc}{}^r$ : ratio of linear polymer degree of polymerization to that of the BBPS-r-PMMA side chains.  $N_{sc}{}^m$  is the degree of polymerization of BBPS-m-PMMA side chain.  $N_{sc}{}^r$  is the degree of polymerization of BBPS-r-PMMA side chain.

Polymer	M <sub>n</sub> (kg/mol)	$N_m$	Ð	$N_m/N_{sc}^m$	$N_m/N_{sc}^r$
PS3	3.10	29.8	1.05	0.84	1.1
PS17	16.9	162	1.02	4.6	6.0
PS59	59.3	570	1.05	16	21
PS120	120	1152	1.04	33	43
PMMA2	1.94	19.4	1.09	0.56	0.72
PMMA10	9.71	97.1	1.04	2.8	3.6
PMMA55	55.1	551	1.06	14	20
PMMA106	106	1060	1.15	28	39

# Instrumentation.

<sup>1</sup>H Nuclear Magnetic Resonance Spectroscopy (NMR). <sup>1</sup>H NMR spectra were measured on Bruker 600 MHz spectrometers. <sup>1</sup>H NMR chemical shifts were reported in ppm relative to TMS.

Gel permeation chromatography (GPC). GPC was performed using an Agilent Technologies 1200 series module, with THF at 1 mL/min. The module was equipped with three PSS SDV columns in series (100, 1000, and 10,000 Å pore sizes), an Agilent variable wavelength UV/vis detector, a Wyatt Technology HELEOS II multiangle laser light scattering (MALLS) detector ( $\lambda$  = 658 nm), and a Wyatt Technology Optilab reX refractive index (RI) detector. The flow rate of mobile phase THF was 1 mL/min at 40 °C. The mass conversion of the macromonomers was determined by comparing integrated RI peak areas for the bottlebrush copolymer and macromonomer. Bottlebrush copolymer absolute molecular weight was determined by static light scattering, and dn/dc was determined by RI analysis assuming 100 % mass recovery of the bottlebrush copolymer. The GPC results for the NBPS, NBPMMA and BBPS-m-PMMA are presented in **Supporting Information Figure S6**. The GPC results for NBPS-r-PMMA and BBPS-r-PMMA are shown in **Supporting Information Figure S7**.

Static Contact Angle Measurements. Static contact angle measurements were carried out with a Krüss Instruments Drop Shape Analyzer DSA 100 at ambient conditions. Contact angles were measured 30 seconds after contact with testing. The reported contact angles reflected average values with standard deviation from at least three measurements from different regions of each sample.

Determination of Surface Energy. The surface energies of target polymers were measured with Krüss Instruments Drop Shape Analyzer DSA 100 at inert atmosphere. For polymers at room temperature (20 °C), the surface energies were determined with contact angle measurement of water and diiodomethane with OWRK model. For surface energy measurements at 150 °C, a pendant drop of polymer was created in a sealed chamber flushed with nitrogen. The surface energy was determined by the Young-Laplace equation. The surface energy was recorded continuously until stable plateau was obtained, and the reported surface energy reflected average values from the plateau.

Ellipsometry. The thicknesses of the films were measured by a spectroscopic imaging ellipsometry (Nanofilm Technologie GmbH, Goettingen, Germany). The incident angle was set to  $70^{\circ}$ , and a multi-wavelength measurement (360-1000 nm) was employed to measure the phase shift  $\Delta$  and the ratio of reflection coefficients of p and s polarizations  $\Psi$  over a region of interest. The refractive index, extinction coefficient, and film thicknesses were determined by fitting to an optical model using the Cauchy function  $n(\lambda)=A_n+B_n/\lambda^2$ , where  $A_n$  and  $B_n$  are Cauchy constants,  $\lambda$  is the incident wavelength (nm). Typical values of  $A_n$  and  $B_n$  are 1.50 and 0.007 for PS and 1.56 and 0.004 for PMMA, respectively.

Polarized Optical Microscopy. Optical micrographs were captured by a Zeiss Axioplan2 polarizing optical microscope (POM) operating in reflectance mode. POM images are shown in the Supporting Information Figures S8 – 11.

Film Preparation. The bottlebrush copolymers and linear PS or PMMA were dissolved in chlorobenzene at a total composition of 5 wt % solids. The mass ratio of bottlebrush copolymer to linear polymer was 1:9 in all cases. Films were cast by flow coating polymer blend solutions onto pre-cleaned silicon wafers. The gap height was fixed at 200 μm, and 20 μL solution was added into the gap for each film. Most film thicknesses ranged from 100 to 150 nm (see **Supporting Information Tables S1 – S4**). Thermal annealing was performed inside a nitrogen filled glovebox at 150 °C for 2 or 7 days.

Time of Flight Secondary Ion Mass Spectrometry (ToF-SIMS). Positive high mass resolution depth profiling was performed using a ToF-SIMS NCS instrument, which combines a ToF.SIMS5 instrument (ION-TOF GmbH, Münster, Germany) and an in-situ Scanning Probe Microscope (NanoScan, Switzerland) and is maintained by the Shared Equipment Authority (https://research.rice.edu/sea/) from Rice University. A bunched 30 keV  $Bi_3^+$  ions (with a measured current of 0.2 pA) was used as primary probe for analysis (scanned area  $90 \times 90 \ \mu m^2$ ), and sputtering was performed using  $Ar_{1500}^+$  ions at 10 keV with a typical current around 0.6 nA and rastered area of  $500 \times 500 \ \mu m^2$ . The beams were operated in non-interlaced mode, alternating 2 analysis cycles and 1 sputtering cycle (corresponding to 1.63 s) followed by a pause of 5s for charge compensation with an electron flood gun. An adjustment of the charge effects has been operated using a surface potential of 6.9 V. During the depth profiling, the cycle time was fixed to  $200 \ \mu s$  (corresponding to  $m/z = 0 - 3649 \ a.m.u$  mass range).

Determination of depth-dependent bottlebrush copolymer compositions in blend films. The calibration procedure for BBPS-m-PMMA blends was described in our previous study.<sup>29</sup> As for

the calibration of BBPS-r-PMMA, we first measured the C<sub>7</sub>H<sub>7</sub><sup>+</sup>/C<sub>2</sub>H<sub>3</sub>O<sub>2</sub><sup>+</sup> ion intensity ratio for a series of miscible, low molecular weight PS/PMMA blends at known mass ratios. Specifically, we analyzed blends of BBPS-r-PMMA with PMMA2 ( $M_n = 1.94 \text{ kg/mol}$ ) and PS3 ( $M_n = 3.10 \text{ kg/mol}$ ) over a range of blend compositions. For each blend, we determined the average C<sub>7</sub>H<sub>7</sub><sup>+</sup>/ C<sub>2</sub>H<sub>3</sub>O<sub>2</sub><sup>+</sup> ion intensity ratio through ToF-SIMS depth profiling measurements. These ion-intensity ratios were found to vary linearly with the BBPS-r-PMMA-to-PS or BBPS-r-PMMA-to-PMMA mass ratios. We produced a linear fit of the secondary ion intensity ratio as a function of BBPS-r-PMMA mass concentration and used this to determine the bottlebrush copolymer mass concentrations using measured secondary ion intensity ratios from the blend films studied. The resulting mass compositional distributions were integrated and normalized with respect to the known bottlebrush content in each film, 10 wt %. The linear PMMA homopolymers used in this study contained a diphenylhexyl end group, and therefore each PMMA homopolymer contributed a weak C<sub>7</sub>H<sub>7</sub><sup>+</sup> background ion intensity. This background ion intensity was measured for each PMMA homopolymer and subtracted from the measured C<sub>7</sub>H<sub>7</sub><sup>+</sup> ion intensity from the blend films. Additional details including the secondary ion ratios measured during calibration and linear relationship between the secondary ion ratio and film composition are provided in the **Supporting Information.** The measured ion intensity ratios along with a linear fit to each dataset are presented in the Figures S16 and S17 and Supporting Information Tables S5 and S6.

Determination of normalized interfacial excesses. The normalized surface, substrate, and total excesses were determined through integration of the depth-dependent bottlebrush copolymer compositions:<sup>43,44</sup>

$$Z_{N \, tot}^* = Z_{N \, surf}^* + Z_{N \, sub}^* = \left\{ \int_0^{\frac{h}{2}} [\varphi(z) - \varphi^0] dz + \int_{\frac{h}{2}}^h [\varphi(z) - \varphi^0] dz \right\} / h$$

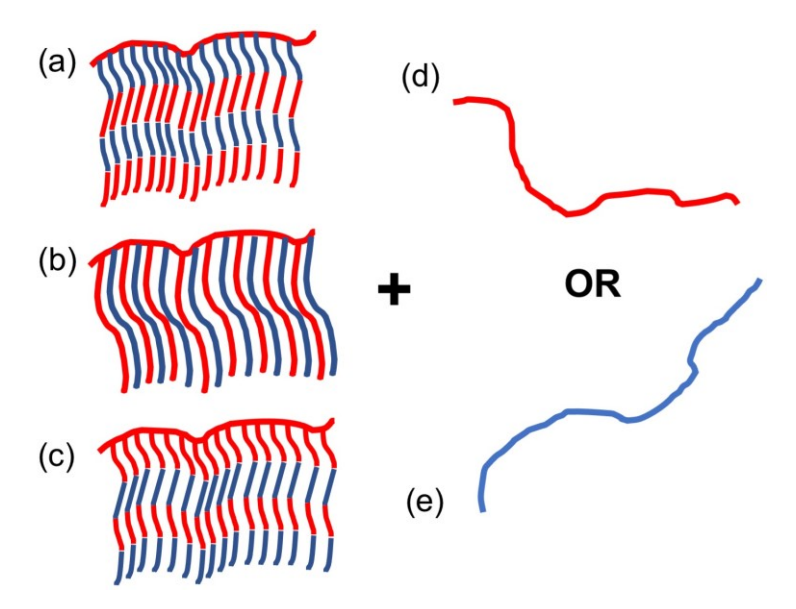
where  $Z_N *_{surf}$ ,  $Z_N *_{sub}$  and  $Z_N *_{tot}$  are the normalized surface, substrate, and total excesses, respectively. h is the thickness of the film, z = 0 corresponds to the film-air interface, and z = h the film-substrate interface.  $\varphi(z)$  is the weight fraction of bottlebrush copolymer in the film as a function of depth z.  $\varphi^0$  was taken to be the composition of bottlebrush copolymer in the middle of the film. The integrations were performed over the surface and substrate regions of the film, which correspond to the regions of z = 0 to h/2 for the surface and z = h/2 to h for the substrate.

# **Simulation Model and Method**

We developed a field-theoretic model to investigate the equilibrium mixing behavior in films containing blends of bottlebrush copolymers and linear homopolymers. The model is a generalization of our previous work related to blends of bottlebrush and linear homopolymer. 15,29 The chains of the linear polymer and the bottlebrush polymer were modeled to be flexible continuous paths containing Kuhn segments. Thin films were modeled by masking functions 45,46 with prescribed (and fixed) density profiles representing substrate (subscripted as *sub*) and air (subscripted as *air*) surfaces. The interaction between the dissimilar polymer segments and between the polymer segments-interfaces (both the substrate as well as air) were modeled as short-ranged interactions. The strengths of the respective interactions were characterized by Flory-Huggins parameters, which qualitatively captured the wetting conditions at the interface between polymer-air and polymer-substrate.

To understand surface segregation in the films, we simulated model bottlebrushes having side chains grafted at regular intervals that contain Kuhn segments of either S (representing styrene) or

M (i.e., methyl methacrylate), blended with either S or M linear homopolymers (Scheme 2). In our effort to reduce the number of interaction parameters, backbones of the bottlebrushes were assumed to contain Kuhn segments of S only. The qualitative trends in segregation of bottlebrush did not change when M was considered as the backbone instead of S, within the interaction parameter space explored here for non-selective surfaces. The bottlebrush copolymer architectures and the homopolymer chain model parameters were chosen to represent the experimental system as faithfully as possible. Specifically, the bottlebrush copolymer consisted of a backbone with  $N_b$ statistical segments of S. For BBPS-m-PMMA, the backbone was grafted with  $n_{sc}$  linear side chains of M and S alternately, producing a side chain grafting density of  $n_{sc}/N_b$ . Each side chain consisted of  $N_{sc}$  segments so that the total degree of polymerization of the bottlebrush copolymer was  $n_{sc}N_{sc}+N_b$  as shown in **Scheme 2b**. A similar strategy was used to model BBPS-r-PMMA, the only difference being that each side chain consists of 4 total alternating blocks of S and M. This blocky side chain microstructure was used for BBPS-r-PMMA because the continuous Gaussian chain approximation put a restriction on the lower limit of the block size. Moreover, the goal was to study the effects of side chain microstructure by varying nature of ends and joints. So, we selected two possible models for BBPS-r-PMMAs with either S end segments (i.e., joints involve M segments) or M end segments (i.e., joints are formed by S segments) as shown in Scheme 2a and 2c, respectively. Each linear homopolymer was made up of  $N_m$  segments of either S or M.



**Scheme 2.** Illustration of bottlebrush copolymer and homopolymer architectures studied in this work (a) BBPS-r-PMMA with S end segments; (b) BBPS-m-PMMA; (c) BBPS-r-PMMA with M end segments; (d)  $N_m$  segments of linear homopolymer S; (e)  $N_m$  segments of linear homopolymer M. The bottlebrush copolymer is blended with either S or M homopolymer in this study. Red color indicates the S component and blue color indicates the M component.

The Flory-Huggins parameter between dissimilar polymer segments was chosen to be similar to our previous work.<sup>29</sup> Our choice for the interaction parameter was motivated by the fact that a very low interaction parameter led to an athermal system and a very high interaction parameter led to microphase separated morphologies of the copolymers. Neither of these phenomena were observed in our experiments. For most cases, the interaction parameter between the polymer segments and the substrate/air-interface was set to zero. However, we systematically varied the interaction parameter of the polymer segments with the interface to get a deeper understanding of the role of bottlebrush side chain microstructure on the segregation behavior.

SCFT based simulations were used to understand the underlying physics behind the qualitative trend observed in the experiment. Hence, we chose continuous Gaussian chain model for all the polymer chains. A more sophisticated model representing the bottlebrush backbone either as rigid<sup>3</sup> or semi-flexible<sup>24</sup> may be necessary for quantitative modeling. A general recipe for statistical field theory of the model can be found elsewhere. Standard saddle-point approximation was invoked and the modified diffusion equations were solved by a pseudo-spectral algorithm. The numerical calculations were performed using PolySwift++.

### **Results and Discussion**

We synthesized bottlebrush copolymers with mixed or random side chains, termed BBPS-*m*-PMMA and BBPS-*r*-PMMA and shown schematically in **Figure 1**. BBPS-*m*-PMMA contained both PS and PMMA side chains while BBPS-*r*-PMMA contained PS-*r*-PMMA random copolymer side chains. The styrene and MMA contents were 47 and 53 wt % for both bottlebrush copolymers. The degrees of polymerization of the backbones for each bottlebrush copolymer were similar (44 and 54 for BBPS-*m*-PMMA and BBPS-*r*-PMMA, respectively), and BBPS-*m*-PMMA had slightly longer side chains compared with BBPS-*r*-PMMA (4.1 and 3.3 kg/mol, respectively). Additional details on these samples are provided in **Table 2**.

To understand the effects of side chain microstructure on surface activity, we solution-cast blends of each bottlebrush copolymer with linear PS or PMMA *via* flow coating. Film thicknesses were measured by ellipsometry and found to be between 100 and 200 nm for most of the films. We also analyzed the film morphology by optical microscopy, shown in **Figures S8** – **S11**, to check for uniformity and possible dewetting. All films were uniform after annealing, except for blends of BBPS-*r*-PMMA in PS17. These samples were excluded from further analysis. To

determine the distribution of bottlebrush additives in the films, we utilized ToF-SIMS depth profiling analyses. We analyzed the  $C_7H_7^+$  and  $C_2H_3O_2^+$  secondary ion signals, which corresponded to PS and PMMA, respectively. The raw secondary ion intensities were converted to mass fractions through calibration using fully miscible blends of PS and PMMA. The calibration process is described in the Experimental Section and the **Supporting Information**.

Representative results of ToF-SIMS analyses of bottlebrush blends with linear PS or PMMA are shown in Figure 2, and results for all blends studied are shown in the Supporting Information Figures S18 – S19. In the as-cast films, we observed strong segregation of both bottlebrushes to the film surface in all blends except for those with PS3 and PMMA2. We previously demonstrated that segregation of bottlebrush additives to film interfaces depends strongly on the relative degrees of polymerization (DP) of the linear polymer and bottlebrush polymer side chains, and segregation was observed when the linear polymer DP exceeds twice that of the bottlebrush side chains. Strong enrichment at the polymer-air interfaces was observed when the linear polymer molecular weight was equal or higher than 17k (i.e.  $N_m/N_{sc}$  ratio was equal or higher than 2.8) for all the as-cast blends. This is due, in part, to entropic effects which preferentially drive branched polymers to film interfaces, as has been discussed in prior studies studies.  $^{15,17,43}$ 

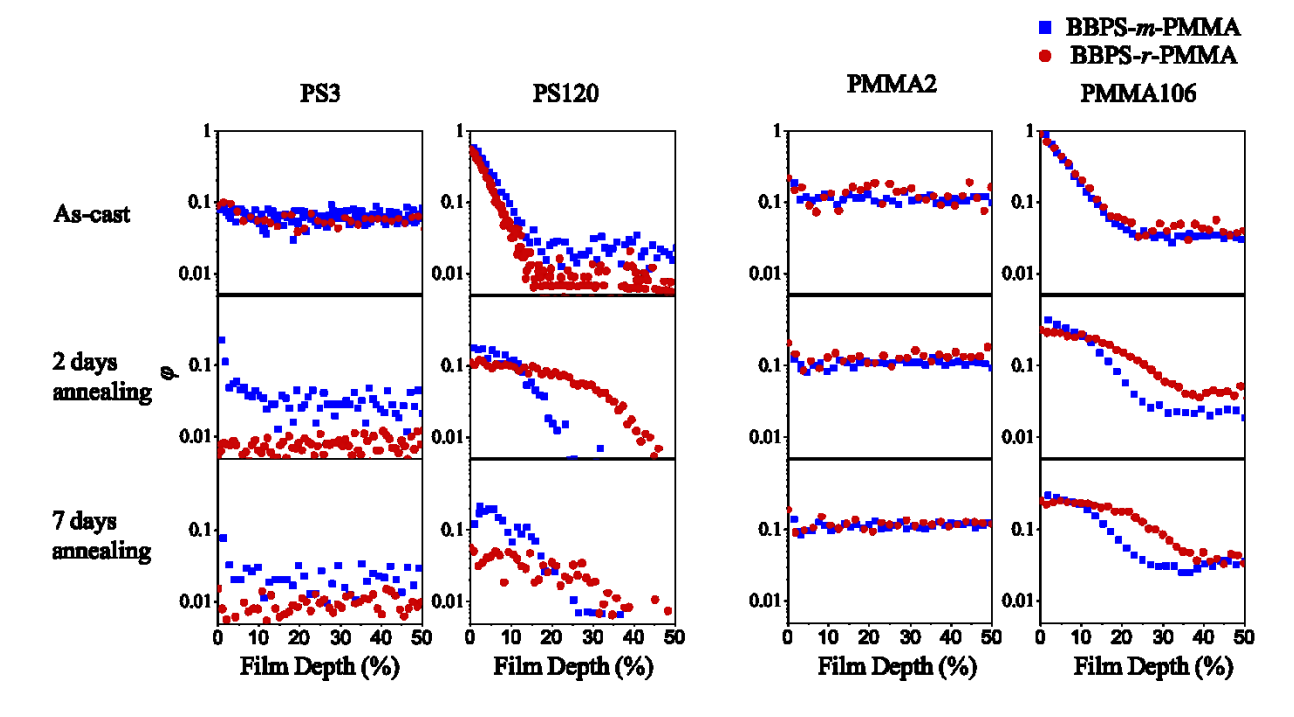


**Figure 2.** BBPS-*m*-PMMA and BBPS-*r*-PMMA mass composition  $\varphi$  as a function of film depth in blend films with linear PS/PMMA. The polymer—air interface and middle of the film are at 0 and 50% film depth, respectively.

After thermal annealing, the surface enrichment decreased for all blends with  $N_m/N_{sc} > 3$ . As shown in **Figure 2**, the bottlebrush polymers dissolved back into the film and/or migrated to the bottom of the film during annealing. After approximately 2 days of thermal annealing the blends were near thermal equilibrium since only small changes to the vertical concentration profile were observed with further annealing for up to 7 days. While the surface enrichment of both additives was similar, we did observe some differences in the distribution of the additives after annealing. The concentration of bottlebrush at the top of the film (film depth 0%) after annealing was generally higher for the mixed bottlebrush additives (see PS3, PS120, and PMMA106 after 2 days and 7 days annealing). However, the concentration of the mixed bottlebrush additive dropped off more strongly with film depth compared with the random bottlebrush additive. This suggests

that BBPS-*m*-PMMA has a relatively lower miscibility with linear PS and PMMA or a relatively stronger affinity to the film air interface compared with BBPS-*r*-PMMA. The normalized substrate excess, normalized total excess, and additive concentration are shown in **Supporting Information Figures S20 – S22**.

To quantitatively compare the surface enrichment for BBPS-m-PMMA and BBPS-r-PMMA additives, we calculated the surface, substrate, and total excesses of bottlebrush copolymer additive in each blend films as shown in **Figure 3** and **Figure S20** – **S22** in **Supporting Information**. These were normalized by the film thickness to eliminate the influence of thickness variations of the films. In both as-cast and annealed films, the normalized surface excess was lowest for the smallest  $N_m/N_{sc}$  values ( $N_m/N_{sc} < 1$ ), and increased with  $N_m/N_{sc}$ . For most samples, the surface excess approached a plateau or maximum value near  $N_m/N_{sc}$  values of approximately 10. Comparing as-cast and annealed samples, the surface excess decreased with longer annealing time, particularly for BBPS-r-PMMA with PS after 7 days annealing.

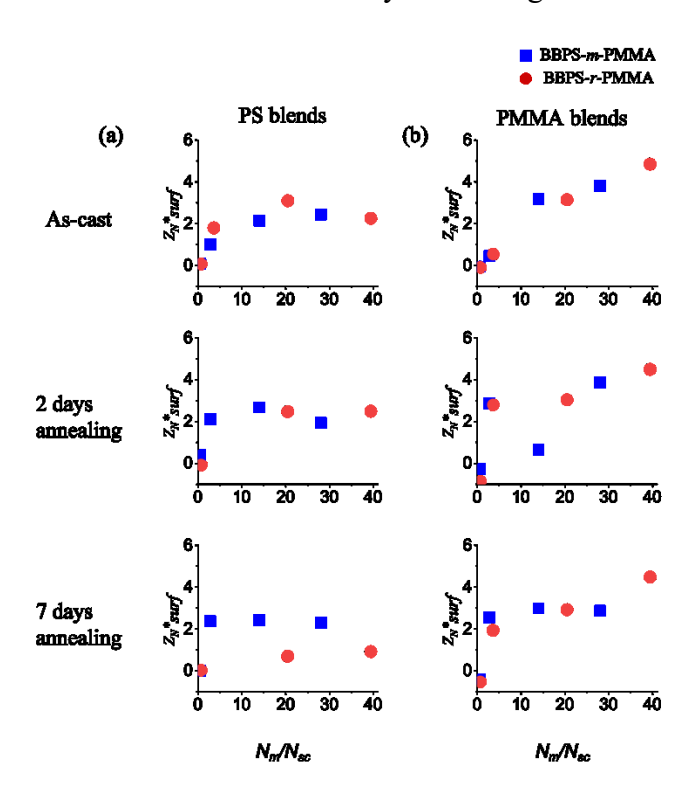


**Figure 3.** Normalized surface excess  $Z_N *_{surf}$  at the film-air interface for blends in (a) PS and (b) PMMA as a function of  $N_m/N_{sc}$ .

The surface excesses measured for BBPS-m-PMMA and BBPS-r-PMMA bottlebrush additives were similar for most blends. To understand differences between these additives, we measured the surface energies of each bottlebrush polymer at room temperature (20 °C) via static contact angle and at the annealing temperature (150 °C) by pendant drop method. 150 °C was above the glass transition temperature  $(T_g)$  of either component, and representative pendant drop images of these two bottlebrush copolymers can be found in Supporting Information Figure S23. BBPS-m-PMMA had a higher surface energy at both temperatures, with a more significant difference at elevated temperatures ( $\Delta y = 7.09 \text{ mN/m}$  at 150 °C compared with 1.48 mN/m at 20 °C). This is surprising given the similar surface enrichments observed and suggests that miscibility differences with the linear polymer may be playing an important role. We also performed water contact angle measurements on blend films with either BBPS-m-PMMA or BBPS-r-PMMA bottlebrush additives in linear PS and PMMA (Supporting Information Figures S24 – S25). For blends with linear PMMA, the additives increased the surface water contact angle, indicating that the surface was more hydrophobic due to the presence of the additive. Consistent with the ToF-SIMS surface excess measurements, the largest change in the surface contact angle was observed in as-cast films, prior to thermal annealing, and a larger effect was observed for the BBPS-m-PMMA additives compared with BBPS-r-PMMA additives. For blends in PS, both bottlebrush additives decreased the surface water contact angle, but there was not a noticeable difference between the additives. This may be due to the relatively small differences in surface segregation for each additive and errors in the water contact angle measurements.

**Table 3.** Surface Energies of BBPS-*m*-PMMA and BBPS-*r*-PMMA at room temperature (20 °C) and elevated temperature (150 °C).

γ (Surface Energy) (mN/m)	20 °C	150 °C
BBPS- <i>m</i> -PMMA	46.14	34.14
BBPS-r-PMMA	44.66	27.05

We utilized SCFT-based modeling to understand the differences between these two bottlebrush copolymers by considering the effects of chain ends and joints. The SCFT allows an efficient modeling of density profiles at thermodynamic equilibrium in inhomogeneous polymeric media such as in the blends of bottlebrush polymers and linear polymers. Furthermore, the SCFT provides information about thermodynamic forces (entropic and enthalpic) resulting from chain ends, joints and their interactions with surfaces as well as the matrix. BBPS-m-PMMA was modelled with alternatively grafted PS and PMMA side chains and was denoted as 1S, as shown in Scheme 2b. The random bottlebrush polymers were modelled as having alternating S and M segments along each side chain and were denoted as either 4S or 4M. 4S had an S segment at the side chain end, while 4M had an M segment at the side chain end. All the bottlebrush copolymers were matched in terms of side chain and backbone degrees of polymerization. This simple model is an approximate representation of the structures of the mixed and random bottlebrush polymers studied experimentally. As in the experiments, the backbone chemistries of the bottlebrush polymers match, and the differences between the polymers are in the microstructures of the side chain. Unlike the experiments, the random side-chain bottlebrushes contained short M or S segments, giving rise to two different types of random side-chain bottlebrushes (4M or 4S). These differ in the chemistry at the joints and chain ends, which impacts the enrichment behavior near interfaces (as shown below).

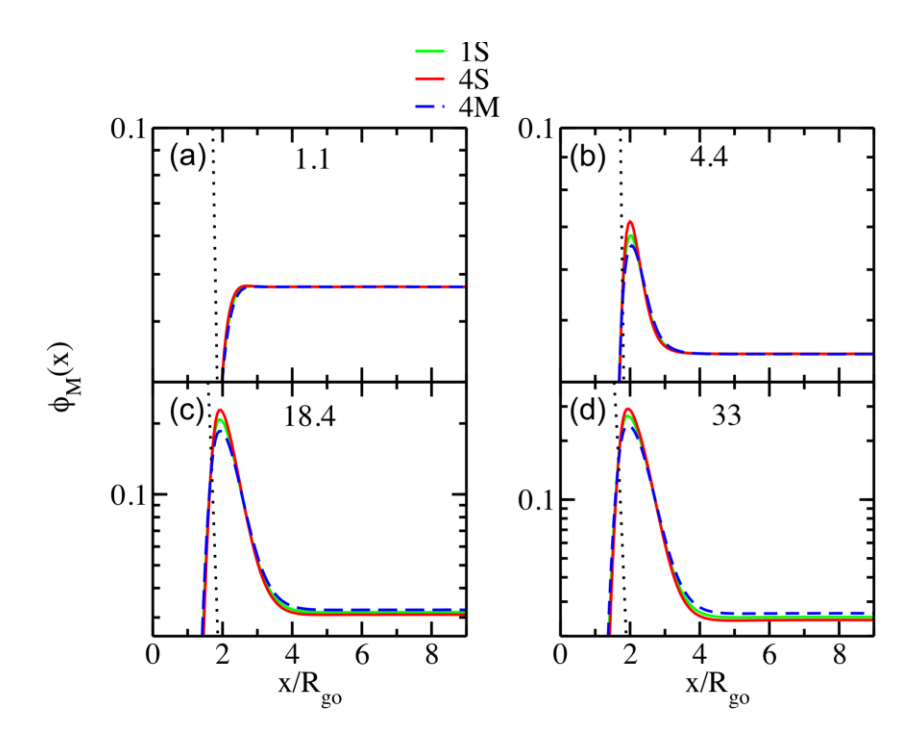
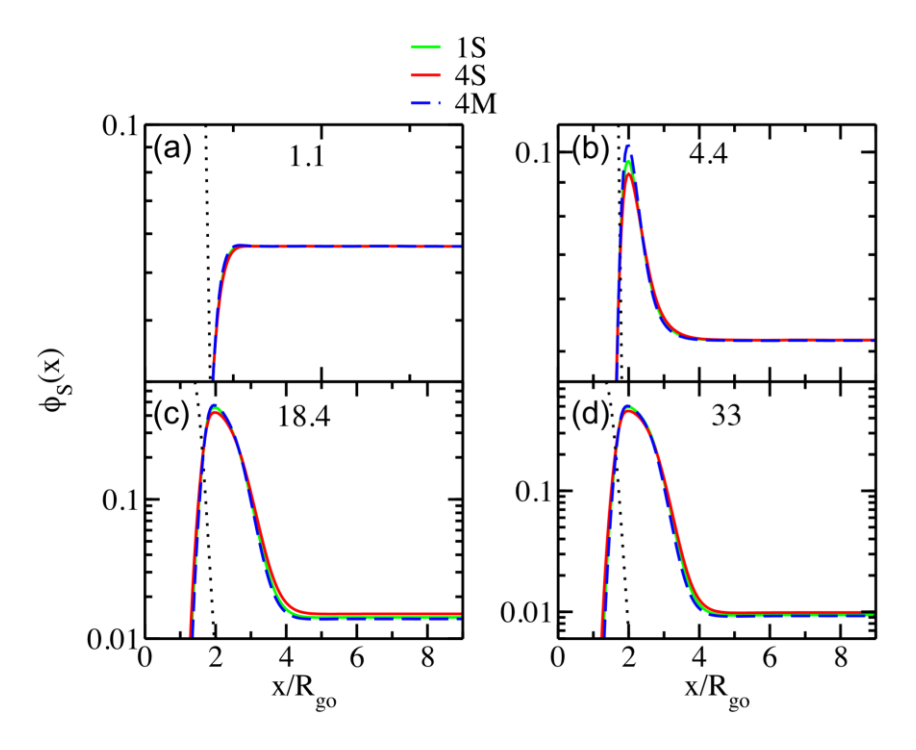


Figure 4. SCFT simulations of polymer blend films for bottlebrush copolymer in PS matrix with (a)  $N_m/N_{sc} = 1.1$ , (b)  $N_m/N_{sc} = 4.4$ , (c)  $N_m/N_{sc} = 18.4$ , and (d)  $N_m/N_{sc} = 33$ . The plots show the equilibrium volume fraction of the minority component (M) in the blend films, reflecting the distribution of the bottlebrush copolymer additive as a function of dimensionless distance from the air surface  $x/R_{go}$ , where  $R_{go}$  is the radius of gyration of the bottlebrush copolymer. Non-selective interfacial interactions ( $\chi_{S-Sub} = \chi_{M-Sub} = \chi_{M-Air} = \chi_{S-Air} = 0$ ) were considered in these simulations. Simulations were executed using  $N_b = 34$ ,  $N_{sc} = 20$ ,  $\chi_{SM} = 0.035$ , bottlebrush copolymer volume fraction  $\varphi = 0.1$ , and film thickness ( $x/R_{go}$ ) = 25.6. Density profiles near one surface are shown here and mirror density profiles are obtained for the other side.

The simulations predict increased surface enrichment with increasing  $N_m/N_{sc}$ , consistent with our experimental observation after 7 days of thermal annealing and prior studies on bottlebrush/linear polymer blends. Furthermore, the simulations showed a difference, although small, in the surface enrichment of the mixed side chain bottlebrush polymer (1S) and the random side chain bottlebrush polymers (4M and 4S). For the films prepared with polystyrene as a matrix,

the strongest surface enrichment was predicted for the 4S bottlebrush and the weakest for the 4M bottlebrush, with degree of segregation for the mixed side chain bottlebrush 1S intermediate between the two random side chain bottlebrushes. A similar trend in segregation of the bottlebrush additives was observed in blends with linear PMMA (Figure 5). However, the strongest surface enrichment was predicted for the 4M bottlebrush, followed by the mixed side chain bottlebrush 1S, and the weakest segregation for 4M. These trends are surprising because the bottlebrush additives with side chain end groups that match those of the linear polymer matrix (4S in PS and 4M in PMMA) are most strongly segregated from the linear polymer matrix, while the mixed bottlebrush copolymer 1S exhibits an intermediate degree of segregation.



**Figure 5**. SCFT simulations of polymer blend films for bottlebrush copolymer in PMMA matrix with (a)  $N_m/N_{sc} = 1.1$ , (b)  $N_m/N_{sc} = 4.4$ , (c)  $N_m/N_{sc} = 18.4$ , and (d)  $N_m/N_{sc} = 33$ . The plots show the equilibrium volume fraction of the minority component (S) in the blend films with non-selective interfacial interactions, reflecting the distribution of the bottlebrush copolymer additive as a

function of dimensionless distance from the air surface  $x/R_{go}$ . All other parameters for the simulations are identical to the ones used for producing **Figure 4**.

Overall, the simulations predict a small but noticeable effect of the side chain microstructures for non-selective interfacial interactions. The trends observed for the films containing the bottlebrush additives demonstrate roles of the bottlebrush joints and side chain end in affecting their surface segregation. In the literature, the effect of entropic contributions on surface segregations has been reported. The "free" end segments and grafted ends (or "joints") of the side chains are entropically attracted and repelled, respectively, from surfaces. 3,19,27,28 An estimate of the entropic surface potential for a joint with three branches in the bottlebrushes can be obtained by using the linear response theory developed by Wu and Fredrickson leading to a surface interaction potential with a prefactor =  $+(\frac{1}{2})*ln(\frac{3}{2})*\xi*k_B*T = +0.203*\xi*k_B*T$ , where  $\xi$  is a correlation length and  $k_BT$  is the thermal energy. Such an estimate needs to be compared with the prefactor of surface potential for a chain end =  $+[1 - ln(2)] * \xi * k_B * T =$  $-0.307 * \xi * k_B * T$ . Based on these estimates, joints are repulsive, and ends are attractive to the surfaces. However, the magnitude of the repulsion of a trifunctional joint is weaker than the attraction of an end so that bottlebrushes containing trifunctional joints should be attractive to the surface due to the fact that attraction of chain ends dominating over the repulsion of the trifunctional joints. These predictions have been recently verified by experimental work by Foster and coworkers, where it was shown that the joints play a secondary role in the surface segregation of branched polymers and the ends mainly drive the surface segregation of branched polymers. 19 However, these theoretical estimations and experimental work focused on conformational entropy of chains and effects of enthalpic interactions have not been considered in detail. SCFT allows us

to precisely estimate both entropic and enthalpic effects. In fact, Wu and Fredrickson conjectured that the enthalpic interactions may either reinforce or compete with these entropic effects.<sup>3</sup> In addition, finite compressibility of polymers has been shown to be important in quantitative comparisons of field theoretical predictions for surface segregation with experimental works,<sup>50</sup> but most of the field theoretical works assume incompressibility in the simulations of surface segregation in blends. Although effects of enthalpic interactions can be included in the SCFT by assuming a chain architecture dependent Flory-Huggins interaction parameter affecting the bulk behavior of blends, such an assumption is unphysical and is not necessary to study surface segregation of branched polymers like bottlebrushes.<sup>50</sup>

For this study, the SCFT simulations were conducted for incompressible polymer blends by considering chain architecture-independent Flory-Huggins interaction parameters for segment-segment and segment-surface interactions. The observed trends in segregation (shown in Figure 4 and 5) reveal that the random side chain bottlebrushes with side chain end segments identical to the linear polymer matrix (i.e., 4S in PS and 4M in PMMA) are the most strongly segregated to the film surface. However, the joints in 4S (or 4M) have MMA (or S) segments, and these are repulsive towards PS (or PMMA). The SCFT simulations therefore demonstrate that a slightly stronger bottlebrush segregation can be obtained by having joints and free ends of the side chains dissimilar and similar, respectively, to the linear polymer matrix. In our experiments, we observed virtually no difference in the segregation behavior of mixed or random side-chain bottlebrush polymers (Figure 3), except in the details of the depth-dependent profiles (Figure 2). This is consistent with the SCFT findings because the experimental samples do not contain segments of M or S near joints or side-chain endgroups (shown in Scheme 1), and therefore there are no significant differences in the joint or side-chain endgroups. We only observed differences in the

depth-dependent distribution, which we hypothesize is due to solubility differences of the two samples.

To understand the influence of substrate preferences, representative comparisons of bottlebrush copolymers (1S, 4S and 4M) in PS blends with different polymer-substrate interactions are displayed in **Figure 6**. Regardless of the interaction parameters, 4S exhibits the strongest enrichment at the polymer-air interface while 4M is the weakest. This demonstrates that substrate preferences influenced bottlebrush surface segregation quantitively, but the qualitative trends remained unchanged. In experiments, we observed a small preference for PMMA at the substrate over PS (see **Supporting Information Figures S18 and S19**).

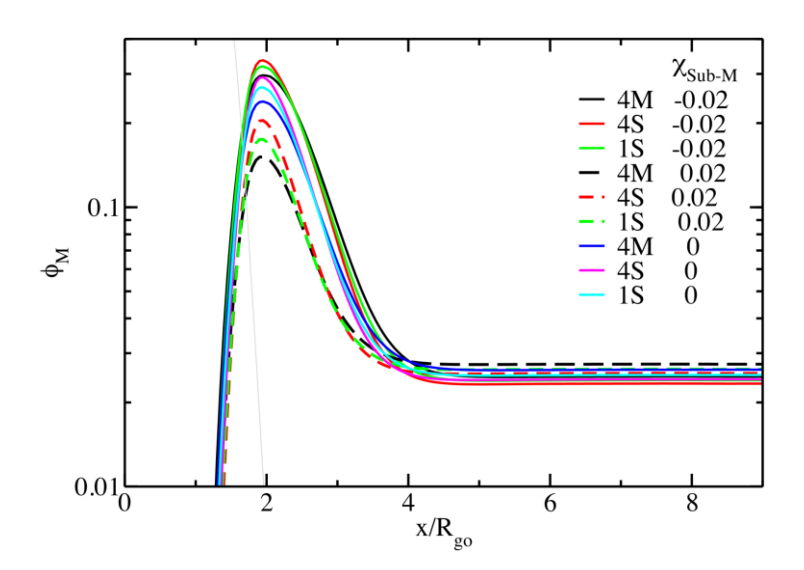


Figure 6. SCFT simulations of polymer blend films for bottlebrush copolymer in PS matrix with  $N_m/N_{sc}=33$ . The plots show the equilibrium volume fraction of the minority component (M) in the blend films, reflecting the distribution of the bottlebrush copolymer additive as a function of dimensionless distance from the air surface  $x/R_{go}$ . Nonselective polymer-air interactions ( $\chi_{M-Air}=\chi_{S-Air}=0$ ) and selective polymer-substrate interactions ( $\chi_{M-Air}\neq\chi_{S-Air}\neq0$ ) were considered in these

simulations. Simulations were executed using  $N_b = 34$ ,  $N_{sc} = 20$ ,  $\chi_{SM} = 0.035$ , bottlebrush copolymer volume fraction  $\varphi = 0.1$ , and film thickness  $(x/R_{go}) = 25.6$ .

This study demonstrates that bottlebrush polymers with either mixed or random copolymer side chains exhibit similar segregation behavior in thin film blends, with only subtle differences in the degree of segregation of the bottlebrush copolymers to film interfaces. Bottlebrush copolymers with mixed side chains are more versatile than those with random copolymer side chains, since many combinations of monomers cannot be easily incorporated into random linear copolymers. For example, it would be difficult to synthesize linear copolymers with styrene and lactic acid repeat units, but mixed bottlebrush polymers with this combination of side chain chemistries and others have been reported and can be synthesized in a one-step polymerization reaction. 51,52 Our work therefore suggests that bottlebrush copolymers with mixed side chain chemistries represent effective and versatile additives for modifying the properties of surfaces and interfaces.

# **Conclusion**

In conclusion, using experiments and simulations we compared the segregation of bottlebrush polymer additives with random (BBPS-r-PMMA) or mixed (BBPS-m-PMMA) side chain microstructures. Both experiments and simulations revealed a small but measurable effect of the side chain microstructure. In experiments, BBPS-m-PMMA additives were observed to segregate slightly more strongly to the film-air interface in blends with PS. Simulations showed differences in the segregation of additives differing in the joint and side chain end-group chemistries. Bottlebrush polymers with joint chemistries that were different from the linear polymer matrix were more strongly segregated to interfaces, while those with joint chemistries that matched that of the linear polymer matrix were more miscible with the linear polymer matrix. The side chain

end-group had a smaller effect on miscibility with the linear polymer matrix and on segregation towards film interfaces than the bottlebrush joint chemistry. This study provides new insights into the phase behaviors of bottlebrush polymers and copolymers blended with linear polymers and suggests that tailoring side chain end-group and joint chemistry may be an effective strategy to design novel bottlebrush additives.

# Acknowledgement

H.M., D.L., J.L., and R.V. acknowledge support from National Science Foundation under Grant No. CMMI-1563008 and Welch Foundation under Grant No. C-1888. T.S.L., A.H.M., and G.E.S acknowledge support from National Science Foundation under Grant No. CMMI-1727517. ToF-SIMS measurements were supported by the National Science Foundation under Grant No. CBET-1626418. ToF-SIMS analyses were carried out with support provided by the Shared Equipment Authority at Rice University. A portion of this research related to the SCFT simulations was conducted at the Center for Nanophase Materials Sciences, which is a DOE Office of Science User Facility at Oak Ridge National Laboratory. This research used resources of the Compute and Data Environment for Science (CADES) at the Oak Ridge National Laboratory, which is supported by the Office of Science of the U.S. Department of Energy under Contract No. DE-AC05-000R22725.

# **Supporting Information**

Detailed description of polymer and bottlebrush synthesis; <sup>1</sup>H NMR and GPC characterization data; optical microscopy and atomic force microscopy analysis of polymer films. ToF-SIMS depth profiling data; polymer film thicknesses; details on methods for ToF-SIMS calibration; plots of

full distribution of bottlebrush additives in linear polymer blends; plots of normalized surface/substrate excess; plots of the additive concentration at the middle of the films; pendant drop images of bottlebrush polymer at elevated temperature.

# References

- (1) Rixens, B.; Severac, R.; Boutevin, B.; Lacroix-Desmazes, P. Migration of Additives in Polymer Coatings: Fluorinated Additives and Poly(Vinylidene Chloride)-Based Matrix. *Polymer* **2005**, *46* (11), 3579–3587. https://doi.org/10.1016/j.polymer.2005.03.041.
- (2) M. Kimani, S.; J. Hardman, S.; R. Hutchings, L.; Clarke, N.; L. Thompson, R. Synthesis and Surface Activity of High and Low Surface Energy Multi-End Functional Polybutadiene Additives. *Soft Matter* **2012**, *8* (12), 3487–3496. https://doi.org/10.1039/C2SM07361G.
- (3) Wu, D. T.; Fredrickson, G. H. Effect of Architecture in the Surface Segregation of Polymer Blends. *Macromolecules* **1996**, *29* (24), 7919–7930. https://doi.org/10.1021/ma9602278.
- (4) Matsen, M. W.; Mahmoudi, P. Segregation of Chain Ends to the Surface of a Polymer Melt. *Eur. Phys. J. E* **2014**, *37* (8), 78. https://doi.org/10.1140/epje/i2014-14078-1.
- (5) Wu, D. T.; Fredrickson, G. H.; Carton, J.-P.; Ajdari, A.; Leibler, L. Distribution of Chain Ends at the Surface of a Polymer Melt: Compensation Effects and Surface Tension. *J. Polym. Sci. Part B Polym. Phys.* **1995**, *33* (17), 2373–2389. https://doi.org/10.1002/polb.1995.090331709.
- (6) Cummings, J.; Lowengrub, J. S.; Sumpter, B. G.; Wise, S. M.; Kumar, R. Modeling Solvent Evaporation during Thin Film Formation in Phase Separating Polymer Mixtures. *Soft Matter* **2018**, *14* (10), 1833–1846. https://doi.org/10.1039/C7SM02560B.
- (7) Zhou, J.; Man, X.; Jiang, Y.; Doi, M. Structure Formation in Soft-Matter Solutions Induced by Solvent Evaporation. *Adv. Mater.* **2017**, *29* (45), 1703769. https://doi.org/10.1002/adma.201703769.
- (8) Cheng, S.; Grest, G. S. Dispersing Nanoparticles in a Polymer Film via Solvent Evaporation. *ACS Macro Lett.* **2016**, *5* (6), 694–698. https://doi.org/10.1021/acsmacrolett.6b00263.
- (9) Howard, M. P.; Nikoubashman, A.; Panagiotopoulos, A. Z. Stratification in Drying Polymer—Polymer and Colloid—Polymer Mixtures. *Langmuir* **2017**, *33* (42), 11390–11398. https://doi.org/10.1021/acs.langmuir.7b02074.
- (10) Zeng, R.; Luo, Z.; Zhou, D.; Cao, F.; Wang, Y. A Novel PEG Coating Immobilized onto Capillary through Polydopamine Coating for Separation of Proteins in CE. *ELECTROPHORESIS* **2010**, *31* (19), 3334–3341. https://doi.org/10.1002/elps.201000228.
- (11) Banerjee, I.; Pangule, R. C.; Kane, R. S. Antifouling Coatings: Recent Developments in the Design of Surfaces That Prevent Fouling by Proteins, Bacteria, and Marine Organisms. *Adv. Mater.* **2011**, *23* (6), 690–718. https://doi.org/10.1002/adma.201001215.
- (12) Kang, G.; Cao, Y. Development of Antifouling Reverse Osmosis Membranes for Water Treatment: A Review. *Water Res.* **2012**, 46 (3), 584–600. https://doi.org/10.1016/j.watres.2011.11.041.
- (13) Tang, L.; Thevenot, P.; Hu, W. Surface Chemistry Influences Implant Biocompatibility. *Curr. Top. Med. Chem.* **2008**, 8 (4), 270–280. https://doi.org/10.2174/156802608783790901.
- (14) Zhang, J.; Clark, M. B.; Wu, C.; Li, M.; Trefonas, P.; Hustad, P. D. Orientation Control in Thin Films of a High-χ Block Copolymer with a Surface Active Embedded Neutral Layer. *Nano Lett.* **2016**, *16* (1), 728–735. https://doi.org/10.1021/acs.nanolett.5b04602.
- (15) Mah, A. H.; Laws, T.; Li, W.; Mei, H.; Brown, C. C.; Ievlev, A.; Kumar, R.; Verduzco, R.; Stein, G. E. Entropic and Enthalpic Effects in Thin Film Blends of Homopolymers and

- Bottlebrush Polymers. *Macromolecules* **2019**, *52* (4), 1526–1535. https://doi.org/10.1021/acs.macromol.8b02242.
- (16) Wei, L.; Caliskan, T. D.; Tu, S.; Choudhury, C. K.; Kuksenok, O.; Luzinov, I. Highly Oil-Repellent Thermoplastic Boundaries via Surface Delivery of CF3 Groups by Molecular Bottlebrush Additives. *ACS Appl. Mater. Interfaces* **2020**, *12* (34), 38626–38637. https://doi.org/10.1021/acsami.0c08649.
- (17) Miyagi, K.; Mei, H.; Terlier, T.; Stein, G. E.; Verduzco, R. Analysis of Surface Segregation of Bottlebrush Polymer Additives in Thin Film Blends with Attractive Intermolecular Interactions. *Macromolecules* **2020**, *53* (15), 6720–6730. https://doi.org/10.1021/acs.macromol.0c00744.
- (18) He, Q.; Wang, S.-F.; Hu, R.; Akgun, B.; Tormey, C.; Peri, S.; Wu, D. T.; Foster, M. D. Evidence and Limits of Universal Topological Surface Segregation of Cyclic Polymers. *Phys. Rev. Lett.* **2017**, *118* (16), 167801. https://doi.org/10.1103/PhysRevLett.118.167801.
- (19) Lee, J. S.; Lee, N.-H.; Peri, S.; Foster, M. D.; Majkrzak, C. F.; Hu, R.; Wu, D. T. Surface Segregation Driven by Molecular Architecture Asymmetry in Polymer Blends. *Phys. Rev. Lett.* **2014**, *113* (22), 225702. https://doi.org/10.1103/PhysRevLett.113.225702.
- (20) Fredrickson, G. H.; Donley, J. P. Influence of Broken Conformational Symmetry on the Surface Enrichment of Polymer Blends. *J. Chem. Phys.* **1992**, *97* (12), 8941–8946. https://doi.org/10.1063/1.463969.
- (21) Fredrickson, G. H.; Liu, A. J. Design of Miscible Polyolefin Copolymer Blends. *J. Polym. Sci. Part B Polym. Phys.* **1995**, 33 (8), 1203–1212. https://doi.org/10.1002/polb.1995.090330806.
- (22) Foster, M. D.; Greenberg, C. C.; Teale, D. M.; Turner, C. M.; Corona-Galvan, S.; Cloutet, E.; Butler, P. D.; Hammouda, B.; Quirk, R. P. Effective χ and Surface Segregation in Blends of Star and Linear Polystyrene. *Macromol. Symp.* **2000**, *149* (1), 263–268. https://doi.org/10.1002/1521-3900(200001)149:1<263::AID-MASY263>3.0.CO;2-0.
- (23) Martter, T. D.; Foster, M. D.; Ohno, K.; Haddleton, D. M. Architecture-Driven Thermodynamic Interactions in Blends of Star-Branched and Linear Poly(Methyl Methacrylate). *J. Polym. Sci. Part B Polym. Phys.* **2002**, *40* (15), 1704–1708. https://doi.org/10.1002/polb.10226.
- (24) Walton, D. G.; Mayes, A. M. Entropically Driven Segregation in Blends of Branched and Linear Polymers. *Phys. Rev. E* **1996**, *54* (3), 2811–2815. https://doi.org/10.1103/PhysRevE.54.2811.
- (25) Mahmoudi, P.; Matsen, M. W. Entropic Segregation of Short Polymers to the Surface of a Polydisperse Melt. *Eur. Phys. J. E* **2017**, *40* (10), 85. https://doi.org/10.1140/epje/i2017-11575-7.
- (26) Hill, J. A.; Endres, K. J.; Mahmoudi, P.; Matsen, M. W.; Wesdemiotis, C.; Foster, M. D. Detection of Surface Enrichment Driven by Molecular Weight Disparity in Virtually Monodisperse Polymers. *ACS Macro Lett.* **2018**, *7* (4), 487–492. https://doi.org/10.1021/acsmacrolett.7b00993.
- (27) Minnikanti, V. S.; Archer, L. A. Entropic Attraction of Polymers toward Surfaces and Its Relationship to Surface Tension. *Macromolecules* **2006**, *39* (22), 7718–7728. https://doi.org/10.1021/ma061377d.
- (28) Qian, Z.; Minnikanti, V. S.; Sauer, B. B.; Dee, G. T.; Archer, L. A. Surface Tension of Symmetric Star Polymer Melts. *Macromolecules* **2008**, *41* (13), 5007–5013. https://doi.org/10.1021/ma8002888.

- (29) Mei, H.; Laws, T. S.; Mahalik, J. P.; Li, J.; Mah, A. H.; Terlier, T.; Bonnesen, P.; Uhrig, D.; Kumar, R.; Stein, G. E.; Verduzco, R. Entropy and Enthalpy Mediated Segregation of Bottlebrush Copolymers to Interfaces. *Macromolecules* **2019**. https://doi.org/10.1021/acs.macromol.9b01801.
- (30) Hariharan, A.; Kumar, S. K.; Russell, T. P. A Lattice Model for the Surface Segregation of Polymer Chains Due to Molecular Weight Effects. *Macromolecules* **1990**, *23* (15), 3584–3592. https://doi.org/10.1021/ma00217a009.
- (31) Hariharan, A.; Kumar, S. K.; Rafailovich, M. H.; Sokolov, J.; Zheng, X.; Duong, D.; Schwarz, S. A.; Russell, T. P. The Effect of Finite Film Thickness on the Surface Segregation in Symmetric Binary Polymer Mixtures. *J. Chem. Phys.* **1993**, *99* (1), 656–663. https://doi.org/10.1063/1.465738.
- (32) Yethiraj, A. Integral Equation Theory for the Surface Segregation from Blends of Linear and Star Polymers. *Comput. Theor. Polym. Sci.* **2000**, *10* (1), 115–123. https://doi.org/10.1016/S1089-3156(99)00064-1.
- (33) Kim, K. H.; Kim, M.; Moon, J.; Huh, J.; Bang, J. Bottlebrush Copolymer as Surface Neutralizer for Vertical Alignment of Block Copolymer Nanodomains in Thin Films. *ACS Macro Lett.* **2021**, 346–353. https://doi.org/10.1021/acsmacrolett.0c00879.
- (34) Kawamoto, K.; Zhong, M.; Gadelrab, K. R.; Cheng, L.-C.; Ross, C. A.; Alexander-Katz, A.; Johnson, J. A. Graft-through Synthesis and Assembly of Janus Bottlebrush Polymers from A-Branch-B Diblock Macromonomers. *J. Am. Chem. Soc.* **2016**, *138* (36), 11501–11504. https://doi.org/10.1021/jacs.6b07670.
- (35) Levi, A. E.; Lequieu, J.; Horne, J. D.; Bates, M. W.; Ren, J. M.; Delaney, K. T.; Fredrickson, G. H.; Bates, C. M. Miktoarm Stars via Grafting-Through Copolymerization: Self-Assembly and the Star-to-Bottlebrush Transition. *Macromolecules* **2019**, *52* (4), 1794–1802. https://doi.org/10.1021/acs.macromol.8b02321.
- (36) Le, A. N.; Liang, R.; Zhong, M. Synthesis and Self-Assembly of Mixed-Graft Block Copolymers. *Chem. Eur. J.* **2019**, *25* (35), 8177–8189. https://doi.org/10.1002/chem.201900520.
- (37) Sanford, M. S.; Love, J. A.; Grubbs, R. H. A Versatile Precursor for the Synthesis of New Ruthenium Olefin Metathesis Catalysts. *Organometallics* **2001**, *20* (25), 5314–5318. https://doi.org/10.1021/om010599r.
- (38) Radzinski, S. C.; Foster, J. C.; Matson, J. B. Preparation of Bottlebrush Polymers via a One-Pot Ring-Opening Polymerization (ROP) and Ring-Opening Metathesis Polymerization (ROMP) Grafting-Through Strategy. *Macromol. Rapid Commun.* **2016**, *37* (7), 616–621. https://doi.org/10.1002/marc.201500672.
- (39) Mei, H.; Mah, A. H.; Hu, Z.; Li, Y.; Terlier, T.; Stein, G. E.; Verduzco, R. Rapid Processing of Bottlebrush Coatings through UV-Induced Cross-Linking. *ACS Macro Lett.* **2020**, *9* (8), 1135–1142. https://doi.org/10.1021/acsmacrolett.0c00384.
- (40) Radzinski, S. C.; Foster, J. C.; Chapleski, R. C.; Troya, D.; Matson, J. B. Bottlebrush Polymer Synthesis by Ring-Opening Metathesis Polymerization: The Significance of the Anchor Group. *J. Am. Chem. Soc.* **2016**. https://doi.org/10.1021/jacs.5b13317.
- (41) Owens, D. K.; Wendt, R. C. Estimation of the Surface Free Energy of Polymers. *J. Appl. Polym. Sci.* **1969**, *13* (8), 1741–1747. https://doi.org/10.1002/app.1969.070130815.
- (42) Kaelble, D. H. Dispersion-Polar Surface Tension Properties of Organic Solids. *J. Adhes.* **1970**, *2* (2), 66–81. https://doi.org/10.1080/0021846708544582.

- (43) Mitra, I.; Li, X.; Pesek, S. L.; Makarenko, B.; Lokitz, B. S.; Uhrig, D.; Ankner, J. F.; Verduzco, R.; Stein, G. E. Thin Film Phase Behavior of Bottlebrush/Linear Polymer Blends. *Macromolecules* **2014**, *47* (15), 5269–5276. https://doi.org/10.1021/ma501070w.
- (44) Kramer, E. J. Depth Profiling Methods That Provide Information Complementary to Neutron Reflectivity. *Phys. B Condens. Matter* **1991**, *173* (1), 189–198. https://doi.org/10.1016/0921-4526(91)90048-J.
- (45) Green, P. F.; Christensen, T. M.; Russell, T. P.; Jerome, R. Surface Interaction in Solvent-Cast Polystyrene-Poly(Methyl Methacrylate) Diblock Copolymers. *Macromolecules* **1989**, 22 (5), 2189–2194. https://doi.org/10.1021/ma00195a033.
- (46) Coulon, G.; Russell, T. P.; Deline, V. R.; Green, P. F. Surface-Induced Orientation of Symmetric, Diblock Copolymers: A Secondary Ion Mass-Spectrometry Study. *Macromolecules* **1989**, *22* (6), 2581–2589. https://doi.org/10.1021/ma00196a006.
- (47) Liu, B.; Narayanan, S.; Wu, D. T.; Foster, M. D. Polymer Film Surface Fluctuation Dynamics in the Limit of Very Dense Branching. *Macromolecules* **2013**, *46* (8), 3190–3197. https://doi.org/10.1021/ma3022986.
- (48) Tzeremes, G.; Rasmussen, K. Ø.; Lookman, T.; Saxena, A. Efficient Computation of the Structural Phase Behavior of Block Copolymers. *Phys. Rev. E* **2002**, *65* (4), 041806. https://doi.org/10.1103/PhysRevE.65.041806.
- (49) Sides, S. W.; Fredrickson, G. H. Parallel Algorithm for Numerical Self-Consistent Field Theory Simulations of Block Copolymer Structure. *Polymer* **2003**, *44* (19), 5859–5866. https://doi.org/10.1016/S0032-3861(03)00606-2.
- (50) Qian, Z.; Minnikanti, V. S.; Sauer, B. B.; Dee, G. T.; Kampert, W. G.; Archer, L. A. Surface Tension of Polystyrene Blends: Theory and Experiment. *J. Polym. Sci. Part B Polym. Phys.* **2009**, *47* (17), 1666–1685. https://doi.org/10.1002/polb.21771.
- (51) Jiang, L.; Nykypanchuk, D.; Ribbe, A. E.; Rzayev, J. One-Shot Synthesis and Melt Self-Assembly of Bottlebrush Copolymers with a Gradient Compositional Profile. *ACS Macro Lett.* **2018**, *7* (6), 619–623. https://doi.org/10.1021/acsmacrolett.8b00273.
- (52) Jiang, L.; Nykypanchuk, D.; Pastore, V. J.; Rzayev, J. Morphological Behavior of Compositionally Gradient Polystyrene–Polylactide Bottlebrush Copolymers. *Macromolecules* **2019**, *52* (21), 8217–8226. https://doi.org/10.1021/acs.macromol.9b01756.

# **TOC Image Only**

